Published in final edited form as:
Neuroimage. 2009 April 1; 45(2): 410–419. doi:10.1016/j.neuroimage.2008.12.014.

Fast optical signal not detected in awake behaving monkeys

Harsha Radhakrishnan[1], **Wim Vanduffel**[1,2,3], **Hong Ping Deng**[1], **Leeland Ekstrom**[1,4,5], **David A. Boas**[1,2,4], and **Maria Angela Franceschini**[1,2,4]

1 *Athinoula A. Martinos Center for Biomedical Imaging, Massachusetts General Hospital, 149, 13th street, Charlestown, MA 02129, USA*

2 *Department of Radiology, Harvard Medical School, Charlestown, Massachusetts, USA 02129*

3 *Laboratorium voor Neurofysiologie en Psychofysiologie, K.U. Leuven Medical School, Campus Gasthuisberg, 3000 Leuven, Belgium*

4 *Harvard-MIT Division of Health Sciences and Technology, 77 Massachusetts Avenue, Cambridge, Massachusetts, USA 02139*

5 *Department of Nuclear Science and Engineering, Massachusetts Institute of Technology, 77 Massachusetts Avenue, Cambridge, Massachusetts, USA 02139*

Abstract

While the ability of near-infrared spectroscopy (NIRS) to measure cerebral hemodynamic evoked responses (slow optical signal) is well established, its ability to measure non-invasively the ‘fast optical signal’ is still controversial. Here, we aim to determine the feasibility of performing NIRS measurements of the ‘fast optical signal’ or Event-Related Optical Signals (EROS) under optimal experimental conditions in awake behaving macaque monkeys. These monkeys were implanted with a ‘recording well’ to expose the dura above the primary visual cortex (V1). A custom-made optical probe was inserted and fixed into the well. The close proximity of the probe to the brain maximized the sensitivity to changes in optical properties in the cortex. Motion artifacts were minimized by physical restraint of the head. Full-field contrast-reversing checkerboard stimuli were presented to monkeys trained to perform a visual fixation task. In separate sessions, two NIRS systems (CW4 and ISS FD oximeter), which previously showed the ability to measure the fast signal in human, were used. In some sessions EEG was acquired simultaneously with the optical signal. The increased sensitivity to cortical optical changes with our experimental setup was quantified with 3D Monte Carlo simulations on a segmented MRI monkey head. Averages of thousands of stimuli in the same animal, or grand averages across the two animals and across repeated sessions, did not lead to detection of the fast optical signal using either amplitude or phase of the optical signal. Hemodynamic responses and visual evoked potentials were instead always detected with single trials or averages of a few stimuli. Based on these negative results, despite the optimal experimental conditions, we doubt the usefulness of non-invasive fast optical signal measurements with NIRS.

Correspondence should be addressed to: Harsha Radhakrishnan, Athinoula A. Martinos Center for Biomedical Imaging, Department of Radiology, Massachusetts General Hospital, 149, 13th street, Rm 2277, Charlestown, MA 02129, Tel: 617-726-4024, Fax: 617-643-5136, Email: harsha@nmr.mgh.harvard.edu.

1. Introduction

Near-infrared spectroscopy (NIRS) has been used for more than a decade to study functional cerebral activation in humans non-invasively (Hoshi and Tamura, 1993; Villringer and Chance, 1997). Similar to fMRI, NIRS is sensitive to the vascular changes following neuronal activity. The vascular responses consist of increases in cerebral blood flow and cerebral blood volume, which cause an increase in oxy-hemoglobin concentration (HbO) and a decrease in deoxy-hemoglobin concentration (HbR). These latter concentration changes are detected by NIRS as changes in light absorbance. While the neuronal electrical signal starts tens of ms after stimulation, the hemodynamic response is delayed and has a latency of a few seconds after stimulation. The spatial and temporal characteristics of the slow optical signals are in agreement and have been validated with fMRI (Huppert et al., 2006a; Huppert et al., 2006b; Sassaroli et al., 2006; Toronov et al., 2007). A less robust but more appealing optical signal is the so-called ‘fast signal’ or ‘event related optical signal’ (EROS) (Gratton et al., 1997b), which detects cortical changes of unclear origin in the ms time scale. The tremendous appeal of the fast signal is due to its short temporal latency, which implies a more direct relationship between neuronal activation and the fast signal compared to the relation that exists with the slow hemoglobin signal. The ability to measure optically both the neuronal and vascular responses non-invasively in humans with reasonable spatial localization puts NIRS in the spotlight as an optimal technique to investigate neurovascular coupling.

Fast light scattering changes possibly induced by cell conformational changes and swelling were originally measured in cell cultures and tissue preparations (Carter et al., 2004; Cohen et al., 1968; Salzberg and Obaid, 1988; Stepnoski et al., 1991; Tasaki and Byrne, 1992; Yao et al., 2005). Detecting back-scattered or cross-polarized light, Rector et al. were able to measure fast optical changes in an animal’s exposed cortex (Rector et al., 2001; Schei et al., 2008). As stressed by Steinbrink et al. (Steinbrink et al., 2005) the existence of fast optical changes in neuronal tissue and the feasibility of using invasive optical methods, like cross-polarized and back-scattered light detection, to detect such changes are not in question. The controversy pertains to the reliability of such measurements obtained with non-invasive optical methods, like NIRS. The first measure of the ‘fast’ signal in humans through intact skin and skull was reported over a decade ago by Gratton et al. (Gratton et al., 1995; Gratton et al., 1997a) using a frequency-domain NIRS system (Imagent, ISS Inc.) and measuring the phase lag (or change in the time of flight) induced by evoked scattering changes (the EROS signal). In the past 10 years, Gratton and co-workers have published a number of very encouraging results with the EROS signal: for example (Bartholow et al., 2001; Gratton et al., 2006; Gratton and Fabiani, 2001; Gratton et al., 1997b; Maclin et al., 2004; Tse et al., 2007). Several groups, including ours, have tried to reproduce Gratton’s measurements (Franceschini and Boas, 2004; Steinbrink et al., 2000; Wolf et al., 2002; Wolf et al., 2003) with moderate success. In contrast with Gratton’s results, these groups have shown, both experimentally and theoretically (with Monte Carlo simulations), that an intensity measurement is better than a phase measurement for detecting the fast signal, because of the better SNR. In a critical work by Steinbrink et al. (Steinbrink et al., 2005), the feasibility of reliably measuring the non-invasive fast optical signal in humans is interrogated, both theoretically and experimentally: the argument being that, based on the estimate of scattering change measured invasively, these changes are too small with respect to instrumental SNR when the partial volume effect is taken into account. For fast signal detection, instrumental SNR is typically increased by averaging a very large number of stimuli and averaging responses across several subjects (Maclin et al., 2007). In addition, physiological noise such as arterial pulsation is reduced using adaptive filters (Gratton and Corballis, 1995; Maclin et al., 2003), and by presenting stimuli in an event-related fashion. Steinbrink et al. (Steinbrink et al., 2005), in addition, increased the SNR significantly by using an optimized NIRS system with considerably higher light power (70–150 mw) delivered to the head than with typical NIRS systems (up to 5–10 mW), thereby reducing the standard error in the average

intensity to 3×10^{-6}, which theoretically was of the order of magnitude of expected scattering induced changes at the head surface. Despite the extremely low noise, they were not able to detect fast optical signals.

To minimize the partial volume effect, and subsequently to further highlight the difficulty of detecting the NIRS fast signal, we performed several NIRS measurements on two macaque monkeys with a recording well with exposed dura over the right primary visual cortex (V1). The head of the animal was restrained by a headpost cemented to the skull, and the optical probe was inserted into the recording well in contact with the dura. This set up mitigates any signal contamination by motion artifacts and avoids signal attenuation from the scalp and skull. These experimental conditions allowed us to perform measurements at a shorter distance from the brain than in human experiments, thereby improving sensitivity to cerebral changes. In different measurement sessions we used a CW and an FD NIRS system and in several sessions we acquired EEG simultaneously with NIRS to detect visual evoked potentials (VEPs). While the NIRS hemodynamic response and the VEP were detected with optimal SNR by averaging few stimuli, we did not detect any reliable fast optical signal even after averaging thousands of stimuli during multiple measurement sessions across the two animals. We conclude that the fast optical signal measured with NIRS is too difficult to obtain to be of any practical utility.

2. Materials and Methods

Subjects, surgical and non surgical preparation, and experimental setup

In this study we performed measurements on two male macaque monkeys (macaca mulatta), M1 (4 years old, 5±0.6 Kg, 7 experimental sessions) and M2 (4 years old, 7±0.56 Kg, 5 experimental sessions). All surgeries and experimental procedures were approved by the Subcommittee on Research Animal Care (SRAC) at the Massachusetts General Hospital, in accordance with NIH guidelines.

Several months prior to the measurements, each monkey was implanted with an MR-compatible plastic headpost covered by dental acrylic (Vanduffel et al., 2001). In addition, the two monkeys had a ‘recording well’ implanted to expose the dura above peripheral V1 of the right visual cortex. The well has a diameter of ~1.8 cm and can host a custom-built optical probe held in position by plastic screws. Figure 1a depicts the plastic headpost and recording well on the monkey’s head. After recovery, each monkey was trained to sit in the ‘sphinx’ position with the head restrained and to fixate on a small dot at the center of a contrast-reversing checkerboard. On the day of the measurement, the monkey was seated in its chair and aseptic procedures applied to avoid infection to the exposed dura. The well was rinsed with sterile saline and cleaned with cotton swabs. Then, the optical probe was inserted into the recording well and held in place using plastic screws (see Fig. 1a). Four additional EEG electrodes were attached to the animal’s head and a pulse oximeter sensor secured to an ear of the animal. The monkey was then placed in a dark chamber in front of a monitor and fixated to the center of the display near-continuously (~90% of the time) for 1–2 hours. A pupil/corneal reflection tracking system (RK-726PCI, Iscan Inc, Cambridge, MA) was used to track the position of the eyes throughout the experiments at a rate of 120 Hz. The eye-tracking system feeds back to a reward system, which automatically delivers apple juice to the animal as a reward when the animal continuously fixated within a 2 deg central fixation window. Figure 1b shows the experimental setup.

Visual Stimulus

For the stimulation, we used a full-field, contrast-reversing radial checkerboard compared to baseline stimulation with a uniform gray screen of mean luminance equal to that of the checkerboard stimulus. We used a block design paradigm with stimuli 20 s on and 20 s off.

Such stimulation, at a different reversal frequency, was previously shown to produce a robust fast optical signal (Gratton et al., 1995; Gratton and Fabiani, 2003; Wolf et al., 2003). The stimulation runs were 6 minutes long and were repeated approximately 6–12 times during each session, as long as the animal cooperated. We used reversal frequencies of 4 Hz in 10 experimental sessions and 7.5 Hz in 4 sessions. In addition, in 2 sessions, random epochs of reversing checkerboards (250 ms single reversal) with ISI of 0.25–3 seconds were presented. Visual stimuli were presented from an LCD screen (maximal resolution of 1024 × 768 pixels, 60 Hz refresh rate) positioned in front of the monkey's eyes at a distance of 46 cm. The monkey was rewarded for maintaining fixation (within a 2 × 2 deg fixation window). Epochs in which the monkeys were not fixating were automatically discarded for data analysis. To synchronize the stimuli onsets with the EEG and NIRS measurements, we used a photodiode attached to a corner of the screen with amplified output sent to both the EEG and NIRS auxiliary inputs. The photodiode detected every transition of the checkerboard pixel under it from black to white and the rising edge of this square wave was used as an onset trigger for both EEG and NIRS fast signal data. The initial rise for each 20 s block was used as an onset to calculate the NIRS slow hemodynamic responses.

NIRS instruments

In different sessions, we performed measurements with a continuous-wave (CW) instrument (CW4, TechEn Inc., Milford, MA) (Franceschini and Boas, 2004), and a frequency-domain (FD) system (Imagent, ISS Inc., Champaign, IL) (Gratton and Fabiani, 2003). Both instruments were optimized to acquire as rapidly as possible in the range of 100 – 250 Hz with optimal SNR. For the CW system 2 laser diodes (690 and 830 nm, emitting ~10 mW) and 5 detectors were used. The lasers modulated at 4 and 6 KHz, respectively, were always on during the acquisition periods and were separated at the detectors offline using a digital bandpass filter with a 100 Hz band-pass frequency. With the FD system, to avoid the noise due to the time-sharing of multiple laser sources, we used only one laser at 830 nm (emitting power of ~3 mW). Data was acquired at 4 ms per data point (250 Hz).

Custom-made probes with diameter 1.7 cm and length 2.5 cm were used. For the CW measurements, the probe had 1 source and 5 detector positions, with SD separations ranging from 0.7 to 1.5 cm, as shown in Fig. 1a. The source fiber was bifurcated at the laser end to connect the two laser sources. For the FD measurements, we used a probe with 1 source and 2 detector positions equidistant from the source at 1.5 cm. From both the FD and CW instruments, auxiliary inputs were used to synchronously acquire the stimulation onsets, the eye-tracking signal, and pulse oximeter SaO_2 and arterial pulsation.

EEG system

For the EEG measurements, we used 5 of the 40 available channels in a monopolar digital amplifier system (NuAmps, Neuroscan labs Inc., USA). We used Ag/Agcl disk-type electrodes (4 mm in diameter, Warner Instruments, Hamden CT, USA) to record the neuronal activity from the visual cortex. The electrode was inserted in the middle of the optical probe (see Fig. 1b) and in contact with the dura when the probe was inserted in the recording well. Four additional Ag/Agcl electrodes (10 mm diameter, Neuroscan labs Inc., USA) were positioned, one below each ear (grounds) and two on the frontal lobe. The right frontal was used as reference electrode and the left frontal marked a second site of acquisition far from the activated visual cortex. We used paste and tape to keep the additional electrodes in position. We verified that the impedance of the electrodes was below 5 KΩ. Data was obtained at a rate of 1 KHz.

NIRS Data Analysis

The optical raw data were processed off-line using in-house software implemented in the MATLAB environment (Mathworks Inc., Sherborn, MA). For the CW system we analyzed

intensity data at 2 wavelengths (690 and 830 nm), while for the FD system we analyzed amplitude data (ac, modulation frequency 110 MHz) and phase shift (ph) data at one wavelength (830 nm). Since the laser light in the CW system is modulated (modulation frequencies 4 and 6 KHz at 690 and 830, respectively) we call the CW intensity as 'ac', as we do for the FD system. In both systems the modulated light offers the advantage of automatically discarding room light;. Apart from the ability to measure a phase shift, there are no other advantages to detecting light at high frequencies with the FD. For the ac we considered percent signal changes $((ac-ac_{mean})/ac_{mean})$ and for the phase shift we considered phase difference $(ph-ph_{mean})$ in deg. To remove the arterial pulsation (heart rate at 2–2.5 Hz) and its higher harmonics, we employed an adaptive filter that fit the amplitude and period of the heartbeat at each point (Franceschini and Boas, 2004). Figure 2 shows the power spectra in dB of the amplitudes (normalized to % changes) and phase (deg) signals with and without the adaptive heart filter for two sessions during 4 Hz stimulation on M1 with the CW (panel a) and FD (panel b) instruments.

With the heart filter we were able to eliminate completely the arterial oscillations and its harmonics from the ac data, while we were not able to reduce them completely from the FD phase data because of the larger noise on this signal. While calculating the power spectra, we performed the FFT analysis by considering all of the intervals with stimuli on and off separately to detect possible response peaks at the stimulation frequency. As a representative case, in Fig. 2 there is no response peak at 4 Hz, and a response peak is not visible even when we average all the sessions together--for either CW or FD measurements. The expected fast signal response in these power spectra figures should have been similar to the EEG response, which is very strong as shown in the power spectra analysis of the EEG signal (see EEG results Fig. 6).

For additional fast signal data analysis, with either the CW or the FD system, raw data were bandpass filtered between 1 and 20 Hz to reduce slow physiological oscillations such as respiration, Mayer waves and slow hemodynamic evoked responses and the high-frequency instrumental noise. To further increase SNR, we did the following for each measurement session: for the CW measurements, data from three detectors at 1 and 1.5 cm separation were averaged together; for the FD measurements, data from the two detectors at a 1.5 cm separation were averaged together. Finally, for each protocol and instrument, data from multiple sessions were block-averaged with thousands of reversal stimulation epochs to achieve a standard error of approximately 0.005%, below the expected amplitude of the fast signal.

By filtering the CW and FD optical data on a lower frequency band (0.01–0.8 Hz), we detected the slow vascular responses to each stimulation block (40-s intervals). Similar to the fast signal analysis, we considered ac percent changes and phase difference. For the CW measurements, in addition to the ac changes at 830 and 690 nm, we also calculated the hemoglobin concentration changes by considering the temporal changes in the intensity at two wavelengths. In this case we used the modified Beer-Lambert law without any path-length correction. Slow signal changes were visible for every stimulation block, as shown in Fig. 3. In order to perform a direct comparison with the fast signal results, we block-averaged the slow responses over all measured runs.

EEG Data Analysis

The EEG measurements were carried out at a sampling frequency of 1 kHz. The EEG signals from each electrode referenced to the right frontal electrode were high-pass filtered at a −3dB cutoff frequency of 3.5 Hz. A notch filter was applied to suppress 60-Hz interference. No heart filter was applied. For each run, we calculated the average VEP response and the Fourier spectra of the response.

Monte Carlo simulations

To predict the magnitude of the effect of a focal scattering change within the brain cortex on our ac and phase measurements, we performed Monte Carlo simulations on 3D structural MRI images of a monkey head (Boas et al., 2002). The Monte Carlo simulations also allowed us to evaluate the advantage of measuring cortical activation from the exposed dura, as compared to measuring such activation from the head surface. We ran Monte Carlo simulations with sources and detectors either in the recording well or on the surface of the head above the well. For the surface simulations we used source-detector (SD) separations 1.5, 2, 2.5 and 3 cm; for the well simulations, 0.5, 1 and 1.5 cm. Fig. 4 shows a slice of the anatomical MRI with source and detector positions in the head surface and in the recording well (indicated in the figure in gray) above V1. The head is segmented into four tissue types (scalp and skull, cerebral spinal fluid, gray matter and white matter; see (Dale et al., 1999)). With the available MRI images we could not separate skull from scalp and therefore considered the two as scalp. For the four tissue types, we used the same optical properties as in (Franceschini and Boas, 2004). To simulate the fast signal, we ran Monte Carlo simulations changing the scattering coefficient in an area included in V1 (red area on the gray matter in Fig. 4). Steinbrink et al. (Steinbrink et al., 2005) estimated that the scattering cortical changes associated with the fast signal are no larger than 0.4%. With our direct Monte Carlo simulation (i.e. not utilizing a linear approximation), we cannot directly estimate the magnitude of the ac and phase changes due to such small scattering changes by launching a reasonable number of photons. Hence, in the well configuration, we run simulations with 1%, 5% and 10% V1 scattering changes and extrapolated the results for smaller scattering changes using a linear model. For the surface, we changed scattering in V1 by 10% only, since we could not achieve statistically significant signal changes for smaller scattering changes at the larger SD separations. To estimate measurement noise and assess statistical significance we launched 200,000,000 photons 5 times and considered the variance between the 5 simulation runs. Each simulation took about 8 hours to run on a 64-bit Linux machine using one 2.40GHz Intel(R) Core(TM) processor.

3. Results

Monte Carlo simulations results

In the well configuration, at a 1.0-cm SD separation, we obtained ac changes of 0.5%, 2.1% and 4% for 1%, 5%, 10 % V1 scattering changes (P values $<10^{-4}$), respectively. We verified the linear dependence of the ac changes with respect to the scattering changes and estimated an ac change of 0.19% for a 0.4% scattering change and 0.12% for a 0.2% scattering change. We obtained similar results at 1.5-cm SD separation, with slightly higher P values. These changes in ac are well above our measurement noise level when averaging hundreds of stimuli (ac standard errors ~0.005–0.01%).

For the phase shift, at a 1-cm SD separation, we obtained changes of 0.006 and 0.014 deg for 5and 10 % V1 scattering changes, respectively (P values 2^{-5} and 0.04). We did not achieve any statistical significant phase change for a 1% scattering change. Considering a linear scattering dependence, the extrapolated phase changes due to a 1% scattering change will be 0.001 deg, and only 0.0003 deg for a 0.4% scattering change, both below our experimental errors even after averaging thousand of stimuli (phase standard error ~ 0.001–0.002 deg).

On the surface, by changing the scattering from 1 to 1.1 cm^{-1} (i.e. a 10% change) in V1 we obtained ac changes of 2–2.4% at 2–3 cm SD separations (P values 3^{-4}–0.04). These ac changes are 40% smaller than the ac changes measured in the well. This is due to the smaller partial volume effect for the well which overcomes the smaller path-length from the smaller SD separation (1–1.5 cm for the well vs. 2–3 cm for the surface). Another advantage of the well is that, with shorter SD separations, a larger number of photons reach the detector, thus

decreasing the noise, which in the Monte Carlo simulations translates to much lower P values for the well ac changes with respect to the surface ones. With the large 10% scattering changes, phase changes on the surface were 0.008 deg at 1.5-cm SD separation, and 0.06 deg at 3-cm separation with high but significant P values (0.05); at 2- and 2.5-cm SD separations we did not reach statistically significant changes.

For the surface measurements, by extrapolating the ac results at 10% scattering to the 0.4% scattering changes of the fast signal, we estimated an ac change of less than 0.1% at 2–3 cm SD separations. Such a change is 50% smaller than the change in the well, and the higher noise level expected at the larger distances would make the fast signal measurement from the surface much more challenging than in our experimental setting with an exposed dura.

Visual evoked potential results

Figure 5 shows representative VEP results for the electrode on the well for M2 during a session in which all three stimulation paradigms were employed. The three panels of Fig. 5 show the VEP for the 4-Hz (panel a), 7.5-Hz (panel b) and random stimulation sequences (panel c) obtained by averaging all of the black-to-white reversing epochs on from representative single 6-min runs. The error bars are standard errors. For the 4-Hz stimulation run shown in the figure we averaged 350 reversals; for the 7.5-Hz stimulation run, 675 reversals; and for the random stimulation, 240 reversals. Reversal onsets are indicated by gray vertical bars. For each reversal the VEP signal is composed of three major peaks: a positive peak at ~ 50 ms, a negative peak at ~90 ms and a large positive peak at ~200 ms, which is not present at 7.5-Hz stimulation because of the onset of a new reversal at time 133 ms. The peak latencies of these VEP responses' were consistent across runs, across sessions, and across monkeys. These responses are similar to VEP on macaque monkeys for similar stimuli reported in the literature (Previc, 1986;Schmid et al., 2006).

Figure 6 shows the power spectra of the EEG signal from the electrode on the recording well during the same runs as shown in Fig. 5a and b. The two traces correspond to the FFT for the intervals when the checkerboard was on (black lines) and off (gray lines). For the on intervals, the EEG response at the stimulation frequency is 15–20 dB higher than for the off intervals and has strong harmonics.

Hemodynamic response results

Figure 3 in the Methods section shows examples of the slow hemodynamic response for each stimulation block for the CW and FD measurements at the 4-Hz stimulation. Figure 7 shows the results for CW and FD, averaging all of the runs and measurement sessions for the two monkeys. For the CW measurements, results at the two wavelengths (ac amplitudes) are shown for the 4-Hz and 7.5-Hz reversal stimulation (panels a and b, respectively). Panel c shows the results for ac and phase at 830 nm obtained with the FD measurements at the 4-Hz stimulation. The error bars are standard errors. For the 4-Hz CW we averaged 260 blocks; for the 7.5-Hz CW, and for the FD, we averaged 200 blocks.

The ac signal decreases 2–3% at 830 nm and increases ~1% at 690 nm, which, converted to hemodynamic changes, corresponds to a 2–3 μM×cm (not pathlength corrected) increase of HbO and a ~0.5 μM×cm decrease of HbR. The slow response starts ~1 s after the stimulation onset, increases for the 20 s of stimulation and rapidly decreases 1–2 s after the end of stimulation. The ac results with the FD are noisier than with the CW, because of the higher frequency of modulation of the lasers (110 MHz vs. 4 KHz) and the lower emitted laser power (2 mW vs. 10 mW). The phase shift increases 0.06 deg with increased absorption (in the figure the phase shift is multiplied by 50 for convenience, to be of similar magnitude to the ac changes), and the changes are above the noise level.

Fast signal results

Figure 8 shows the grand averages of the ac data obtained with the CW instrument for the three stimulation protocols, averaging all of the black-to-white reversing epochs. The error bars are standard errors. For the 4-Hz stimulation, we averaged ~10,000 reversal epochs; for the 7.5-Hz stimulation, ~15,000 reversal epochs; and for the random stimulation, 3,300 reversal epochs. Left panels are the results at 830 nm, and the right panels, at 690 nm. Black lines are the results after applying the adaptive heart filter to remove the arterial pulsations; dashed gray lines are the results without applying the heart filter. In panels a, b, c and d the arterial pulsation is reduced by the large average of stimuli, while in panels e and f, where we average only 3,300 stimuli, the arterial pulsation is not completely averaged out. In all cases, applying the adaptive filter reduces the error bars, which for the filtered signals are ≤0.005%. While we expected to see an ac change of 0.1–0.2% from the Monte Carlo results, we do not see any significant fast signal change. In particular, we do not see any changes with periodicity similar to the VEP response (Fig. 5).

Figure 9 shows the results for the frequency-domain measurements where, again, the fast signal is not visible in either the ac or the phase measurements. The unfiltered ac responses have a strong arterial component despite the large number of stimuli averaged (10,000). In most of our experiments the arterial pulsations are larger and have a larger harmonic content for the FD measurements than for the CW measurements (20 dB for FD ac vs. 25 dB for CW ac in Fig. 2, and in general 0.02–0.05% arterial pulsation magnitude in the FD ac vs. 0.01–0.03% magnitude in the CW ac). A possible explanation may be the different dates on which the FD and CW experiments were done, since the dura grew new vessels over time. The phase in Fig. 9b shows the arterial component in both the filtered and unfiltered data, because of the lower success in removing the arterial pulsation from the phase data.

With the FFT analysis averaging sessions and animals, as with Figs. 8 and 9, we noted the absence of any peak at the stimulation frequencies due to a fast signal response (figures not shown since grand average results are very similar to the one reported in Fig. 2 for single session).

4. Discussion and conclusions

With these experiments we tested the feasibility of detecting the fast optical signal with NIRS in an optimal experimental setup. Measuring human subjects, Steinbrink et al. (Steinbrink et al., 2005) reduced the instrumental noise to below estimated fast signal levels by designing an ultra-low-noise CW instrument. In contrast, we used conventional instruments previously used to detect the fast signal and increased the SNR by collecting data closer to the cortex. In fact, the animal model we used, with exposed dura, allowed us to obtain measurements with increased sensitivity to the cortical tissue and a reduced partial volume effect with respect to measurements from the head surface.

We minimized motion artifacts by having the probe fixed to the recording well and the animal's head immobilized by a head-post. The location of the probe was optimal and reproducible across measurement sessions since the recording well was centered above the right primary visual cortex area. The cortical area V1 in the macaque monkeys is about 1200 mm^2 (about 15% of the total cortical area in the macaque) (Hubel, 1995). This means that the activated cortical volume during visual stimulation is large and should significantly affect the measured light pathlength. With Monte Carlo simulations in a 3D segmented head, we estimated the magnitude of ac and phase signal changes due to small scattering changes in V1. We verified that these signal changes were above our instrumental noise, at least for the ac signal. We used radial checkerboard stimulation, which produces strong neuronal and vascular responses, and

tested different paradigms with different stimulation rates to rule out habituation effects. With EEG, we verified that we were able to measure a strong VEP during stimulation.

For the NIRS measurements, we used instruments that have been previously reported by us and by others as being able to measure the fast signal in human subjects. We used visual cortex stimulation paradigms similar to other reported in the literature as able to produce fast signal responses in humans (Gratton et al., 2006; Gratton et al., 1995; Gratton and Fabiani, 2003; Gratton et al., 2001; Maclin et al., 2007; Wolf et al., 2003). We optimized the data collection to minimize the instrumental noise. We detected hemodynamic responses for every stimulation block. Despite these optimal conditions, we were not able to measure any amplitude or phase changes in the 100-ms time scale averaging thousand of stimuli. These results seem to indicate that scattering changes in the cortex, at least in the macaque monkey, are much smaller than 0.4%. These negative findings discourage us from further attempting to measure such signals non-invasively in non-human primates and humans.

With respect to our previously published fast signal results in humans (Franceschini and Boas, 2004), it is possible that stimulus-related motion artifacts contributed to the signal we measured. In that work, we stimulated the somatosensory cortex with stimuli above the motor threshold and we observed that stimulus-related artifacts (very small vibrations that could propagate from the hand that is performing the task to the head of the subject and could change the optical coupling of the probe) could be misinterpreted as fast signals. For this reason, data was discarded based on the 5 criteria we established: (a) The responses at the two wavelengths should be similar, (b) there should be no response during rest periods, (c) responses considering subsets of stimuli should be similar, (d) responses during ipsilateral stimulation should be smaller than responses during contralateral stimulation, and (e) the fast signal should be spatially localized in a small area in the contralateral side. Criteria 1 to 3 identify false responses generated by random noise. Criteria 2 and 4 identify false responses generated by arterial pulsation and other systemic oscillations. Criteria 4 and 5 identify false responses due to stimulus-related motion artifacts, if these motion artifacts affect all of the probe locations in a similar way. Across the three protocols, 40% of the measurements met all of the criteria, 28% of the measurements did not show any response, and 32% of the measurements were discarded because of motion artifacts. The amplitude changes in the measurements that met all of the criteria were extremely small (less than 0.05%), and of the same order of magnitude of the changes due to motion artifacts in the discarded measurements. If the stimulus-related motion artifacts affected the optical coupling of sources and detectors inhomogenously, the resulting changes in intensity could have passed as a fast signal. Also, in our previous work, we used a probe that was made of two independent parts—for the two hemispheres—and the tightness and coupling of sources and detectors to the head was not perfectly homogeneously distributed. We cannot rule out the possibility that these coupling differences may have produced uneven distributed changes in the measured signal.

It seems unrealistic, but it is possible that the fast signal, the origin of which is still unclear, is more difficult to measure in the visual cortex than in the somatosensory cortex. Or that it is simply not present in non-human primates. But because it is such a small signal, and measuring it non-invasively is extremely challenging, we question the utility of NIRS fast signal measurements in general, in agreement with Steinbrink et al. (Steinbrink et al., 2005).

Acknowledgements

This research is supported by the US National Institutes of Health (NIH) grant R01-EB001954, R01-EB000790 and R01-EY017081, the Human Frontiers Science Program (HFSPO), GSKE, IUAP 5/04, and EF/05/014. The Martinos Center is supported by N.C.R.R. grant P41RR14075 and the MIND Institute.

References

Bartholow BD, Fabiani M, Gratton G, Bettencourt BA. A psychophysiological examination of cognitive processing of and affective responses to social expectancy violations. Psychol Sci 2001;12:197–204. [PubMed: 11437301]

Boas DA, Culver J, Stott J, Dunn AK. Three dimensional Monte Carlo code for photon migration through complex heterogeneous media including the adult head. Optics Express 2002;10:159–170.

Carter KM, George JS, Rector DM. Simultaneous birefringence and scattered light measurements reveal anatomical features in isolated crustacean nerve. J Neurosci Methods 2004;135:9–16. [PubMed: 15020084]

Cohen LB, Keynes RD, Hille B. Light scattering and birefringence changes during nerve activity. Nature 1968;218:438–441. [PubMed: 5649693]

Dale AM, Fischl B, Sereno MI. Cortical surface-based analysis. I. Segmentation and surface reconstruction. Neuroimage 1999;9:179–194. [PubMed: 9931268]

Franceschini MA, Boas DA. Non invasive measurement of neuronal activity with near-infrared optical imaging. NeuroImage 2004;21:372–386. [PubMed: 14741675]

Gratton G, Corballis PM. Removing the heart from the brain: compensation for the pulse artifact in the photon migration signal. Psychophysiology 1995;32:292–299. [PubMed: 7784538]

Gratton G, Corballis PM, Cho E, Fabiani M, Hood DC. Shades of gray matter: noninvasive optical images of human brain responses during visual stimulation. Psychophysiology 1995;32:505–509. [PubMed: 7568645]

Gratton G, Fabiani M, Corballis PM, Gratton E. Noninvasive detection of fast signals from the cortex using frequency-domain optical methods. Ann N Y Acad Sci 1997a;820:286–298. [PubMed: 9237461] discussion 298–289

Gratton G, Fabiani M, Corballis PM, Hood DC, Goodman-Wood MR, Hirsch J, Kim K, Friedman D, Gratton E. Fast and localized event-related optical signals (EROS) in the human occipital cortex: comparisons with the visual evoked potential and fMRI. Neuroimage 1997b;6:168–180. [PubMed: 9344821]

Gratton G, Goodman-Wood MR, Fabiani M. Comparison of neuronal and hemodynamic measures of the brain response to visual stimulation: an optical imaging study. Hum Brain Mapp 2001;13:13–25. [PubMed: 11284043]

Gratton G, Fabiani M. The event-related optical signal: a new tool for studying brain function. Int J Psychophysiol 2001;42:109–121. [PubMed: 11587771]

Gratton G, Fabiani M. The event-related optical signal (EROS) in visual cortex: replicability, consistency, localization, and resolution. Psychophysiology 2003;40:561–571. [PubMed: 14570164]

Gratton G, Brumback CR, Gordon BA, Pearson MA, Low KA, Fabiani M. Effects of measurement method, wavelength, and source-detector distance on the fast optical signal. Neuroimage 2006;32:1576–1590. [PubMed: 16872842]

Hoshi Y, Tamura M. Detection of dynamic changes in cerebral oxygenation coupled to neuronal function during mental work in man. Neuroscience Letters 1993;150:5–8. [PubMed: 8469403]

Hubel, DH. Eye, Brain and Vision. Scientific American Library; Harvard Medical School, USA: 1995.

Huppert TJ, Hoge RD, Dale AM, Franceschini MA, Boas DA. Quantitative spatial comparison of diffuse optical imaging with blood oxygen level-dependent and arterial spin labeling-based functional magnetic resonance imaging. J Biomed Opt 2006a;11:064018. [PubMed: 17212541]

Huppert TJ, Hoge RD, Diamond SG, Franceschini MA, Boas DA. A temporal comparison of BOLD, ASL, and NIRS hemodynamic responses to motor stimuli in adult humans. Neuroimage 2006b; 29:368–382. [PubMed: 16303317]

Maclin EL, Gratton G, Fabiani M. Optimum filtering for EROS measurements. Psychophysiology 2003;40:542–547. [PubMed: 14570162]

Maclin EL, Low KA, Sable JJ, Fabiani M, Gratton G. The event-related optical signal to electrical stimulation of the median nerve. Neuroimage 2004;21:1798–1804. [PubMed: 15050600]

Maclin EL, Low KA, Fabiani M, Gratton G. Improving the signal-to-noise ratio of event-related optical signals. IEEE Eng Med Biol Mag 2007;26:47–51. [PubMed: 17672231]

Previc FH. Visual evoked potentials to luminance and chromatic contrast in rhesus monkeys. Vision Res 1986;26:1897–1907. [PubMed: 3617531]

Rector DM, Rogers RF, Schwaber JS, Harper RM, George JS. Scattered-light imaging in vivo tracks fast and slow processes of neurophysiological activation. Neuroimage 2001;14:977–994. [PubMed: 11697930]

Salzberg BM, Obaid AL. Optical studies of the secretory event at vertebrate nerve terminals. Exp Biol 1988;139:195–231.

Sassaroli A, de BFB, Tong Y, Renshaw PF, Fantini S. Spatially weighted BOLD signal for comparison of functional magnetic resonance imaging and near-infrared imaging of the brain. Neuroimage 2006;33:505–514. [PubMed: 16945553]

Schei JL, McCluskey MD, Foust AJ, Yao XC, Rector DM. Action potential propagation imaged with high temporal resolution near-infrared video microscopy and polarized light. Neuroimage 2008;40:1034–1043. [PubMed: 18272402]

Schmid MC, Oeltermann A, Juchem C, Logothetis NK, Smirnakis SM. Simultaneous EEG and fMRI in the macaque monkey at 4.7 Tesla. Magn Reson Imaging 2006;24:335–342. [PubMed: 16677938]

Steinbrink J, Kohl M, Obrig H, Curio G, Syre F, Thomas F, Wabnitz H, Rinneberg H, Villringer A. Somatosensory evoked fast optical intensity changes detected non- invasively in the adult human head. Neurosci Lett 2000;291:105–108. [PubMed: 10978585]

Steinbrink J, Kempf FC, Villringer A, Obrig H. The fast optical signal--robust or elusive when non-invasively measured in the human adult? Neuroimage 2005;26:996–1008. [PubMed: 15961042]

Stepnoski RA, LaPorta A, Raccuia-Behling F, Blonder GE, Slusher RE, Kleinfeld D. Noninvasive detection of changes in membrane potential in cultured neurons by light scattering. Proc Natl Acad Sci USA 1991;88:9382–9386. [PubMed: 1946349]

Tasaki I, Byrne PM. Rapid structural changes in nerve fibers evoked by electric current pulses. Biochem Biophys Res Commun 1992;188:559–564. [PubMed: 1445300]

Toronov VY, Zhang X, Webb AG. A spatial and temporal comparison of hemodynamic signals measured using optical and functional magnetic resonance imaging during activation in the human primary visual cortex. Neuroimage 2007;34:1136–1148. [PubMed: 17134913]

Tse CY, Lee CL, Sullivan J, Garnsey SM, Dell GS, Fabiani M, Gratton G. Imaging cortical dynamics of language processing with the event-related optical signal. Proc Natl Acad Sci U S A 2007;104:17157–17162. [PubMed: 17942677]

Vanduffel W, Fize D, Mandeville JB, Nelissen K, Van Hecke P, Rosen BR, Tootell RB, Orban GA. Visual motion processing investigated using contrast agent-enhanced fMRI in awake behaving monkeys. Neuron 2001;32:565–577. [PubMed: 11719199]

Villringer A, Chance B. Non-invasive optical spectroscopy and imaging of human brain function. Trends Neurosci 1997;20:435–442. [PubMed: 9347608]

Wolf M, Wolf U, Choi JH, Gupta R, Safonova LP, Paunescu LA, Michalos A, Gratton E. Functional frequency-domain near-infrared spectroscopy detects fast neuronal signal in the motor cortex. Neuroimage 2002;17:1868–1875. [PubMed: 12498761]

Wolf M, Wolf U, Choi JH, Toronov V, Paunescu LA, Michalos A, Gratton E. Fast cerebral functional signal in the 100-ms range detected in the visual cortex by frequency-domain near-infrared spectrophotometry. Psychophysiology 2003;40:521–528. [PubMed: 14570160]

Yao XC, Foust A, Rector DM, Barrowes B, George JS. Cross-polarized reflected light measurement of fast optical responses associated with neural activation. Biophys J 2005;88:4170–4177. [PubMed: 15805175]

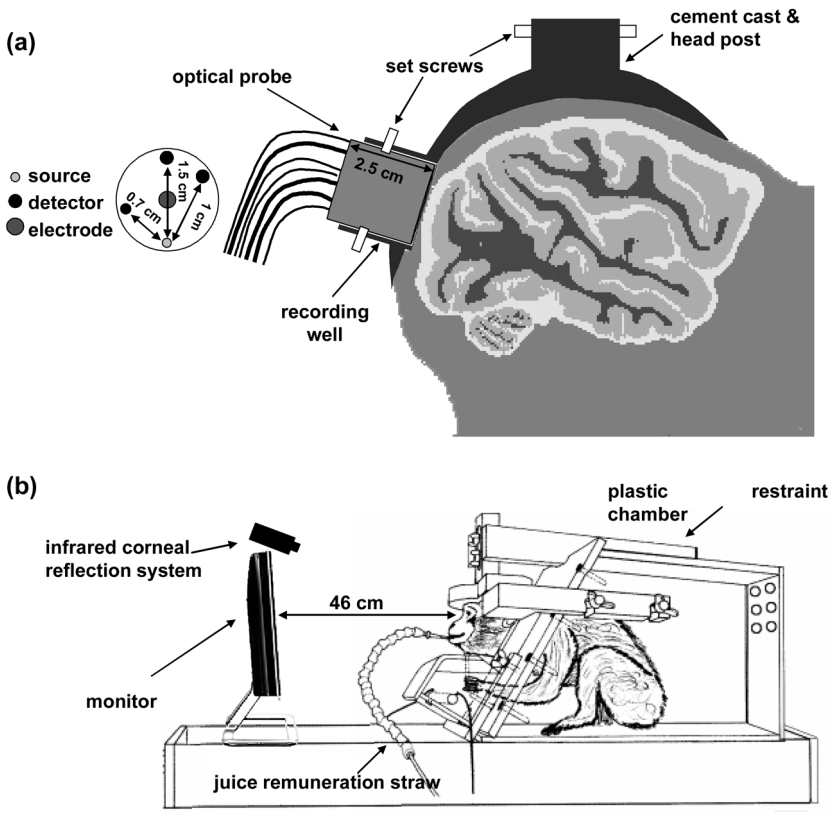

Figure 1.

Panel a shows a schematic of the optical probe inserted in the recording well, the cemented post on the animal head, and the probe geometry with indicated source detector distances. Panel b shows the experimental setup with the animal restrained in a custom-made chamber in front of a monitor.

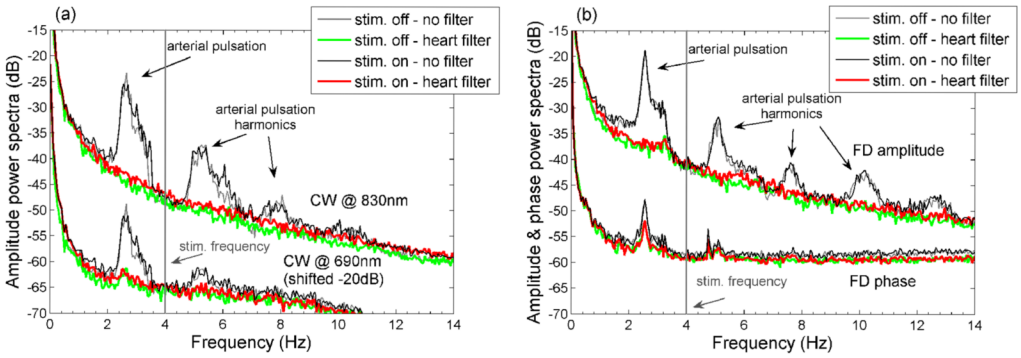

Figure 2.

Power spectra of the CW (panel a) and FD (panel b) data before (black and gray) and after (red and green) the adaptive heart filter. The adaptive filter strongly reduces the arterial pulsations in the 830 nm amplitude data. Because of the lower signal-to-noise at 690 nm and on the phase data the adaptive filter is less effective. While performing the FFTs we divided the data into two subsets, one considering the time intervals with stimulation on (black and red) and one with stimulation off (green and gray). No fast response peak is visible at the stimulation frequency (4 Hz) or its harmonics in the traces with stimulation on.

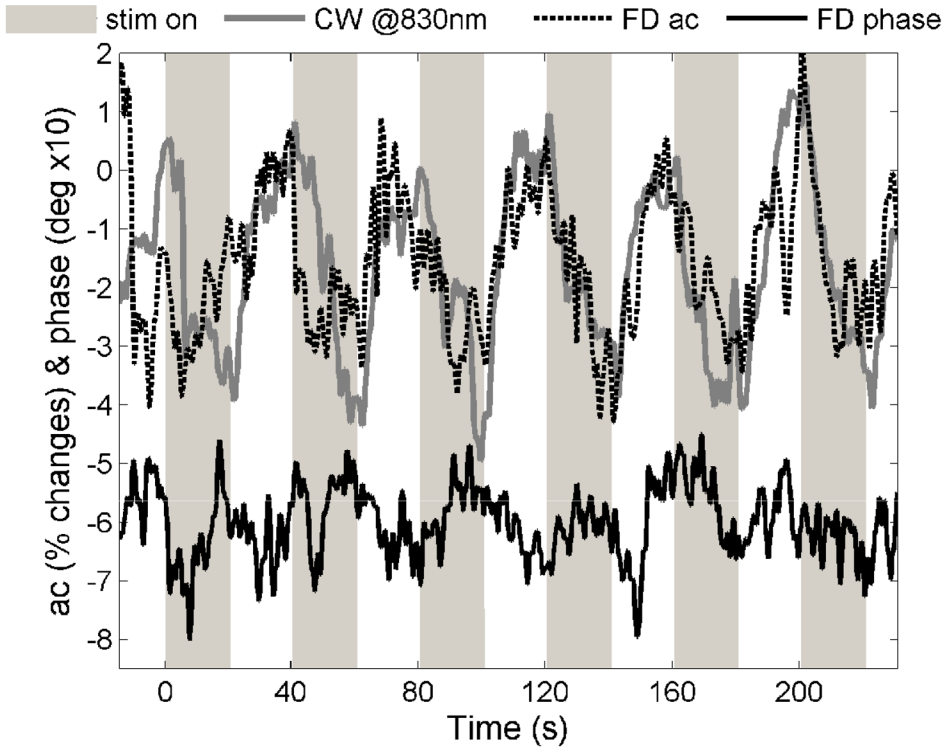

Fig. 3.

Examples of slow vascular responses visible on the raw CW and FD data for each stimulation block. The data are bandpass filtered between 0.01 and 0.8 Hz but not block averaged. The CW and FD data segments in the figure were collected on M1 during two different sessions, stimulating for 20 s at 4 Hz.

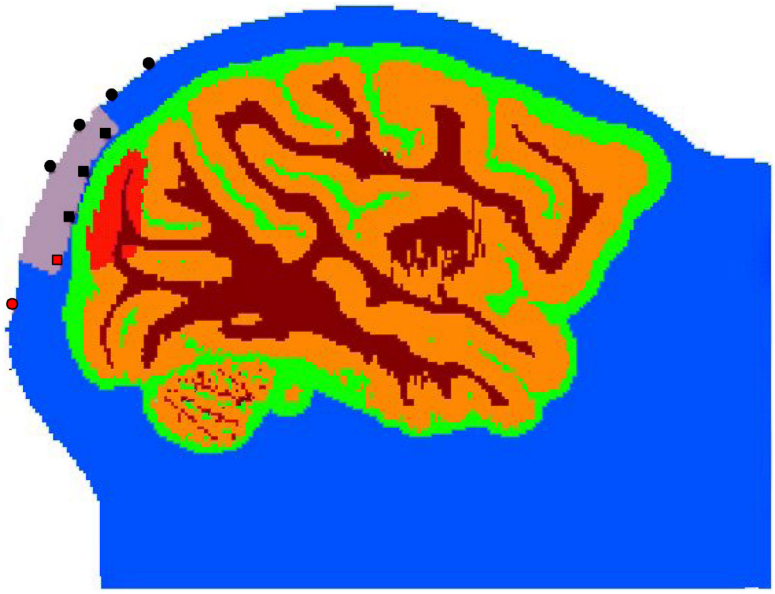

Figure 4.

Slice of the anatomical MRI of a macaque monkey containing sources and detectors. The head is segmented into four tissue types (scalp and skull (blue), cerebral spinal fluid (green), gray matter (orange) and white matter (brown). For the four tissue types, we used the following absorption coefficients: 0.191, 0.026, 0.186, 0.186 cm^{-1}, and the following reduced scattering coefficients: 6.6, 0.1, 11.1, 11.1 cm^{-1} (in this order: scalp and skull, cerebral spinal fluid, gray matter, white matter). The recording well in the figure is indicated by the gray area and the region of V1 for which we change scattering coefficient is indicated in red. Sources (red) and detectors (black) in the head surface are indicated by circles and in the recording well by squares.

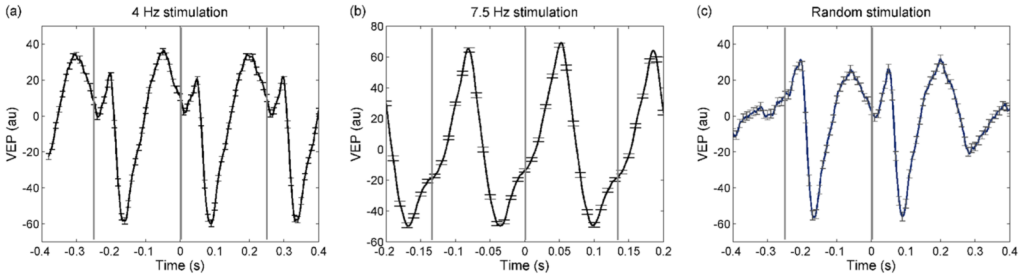

Figure 5.

VEP responses for the 4-Hz (panel a), 7.5-Hz (panel b) and random stimulation sequences (panel c) obtained by averaging representative single 6-min runs during a session on M2. The error bars are standard errors. Please note that the time scale for the 7.5 Hz stimulation is smaller and the y axis larger.

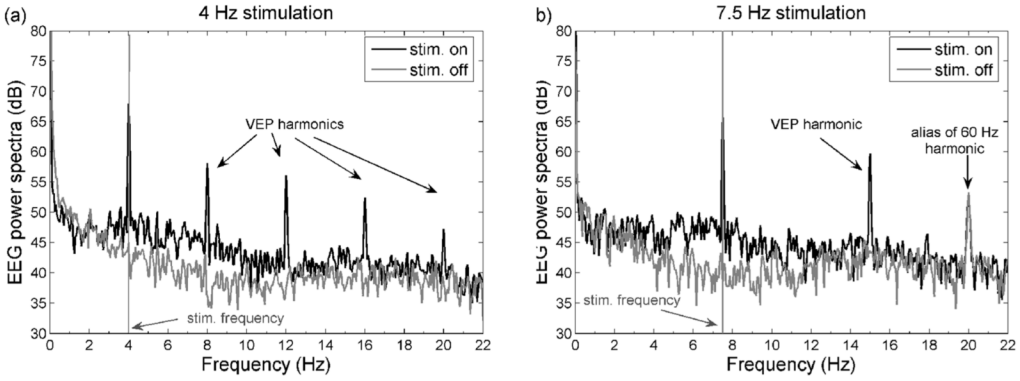

Figure 6.

Power spectra of the EEG data from the electrode on the recording well during representative runs on a session on M2. Panel a: 4 Hz stimulation, panel b: 7.5 Hz stimulation. The random stimulation is not periodic and thus the FFT analysis is not included. While performing the FFTs we divided the data into two subsets, one considering the time intervals with stimulation on (black) and one with stimulation off (gray). The EEG response at the stimulation frequency is 15–20 dB higher when stimulation is on than when it is off and has strong harmonics.

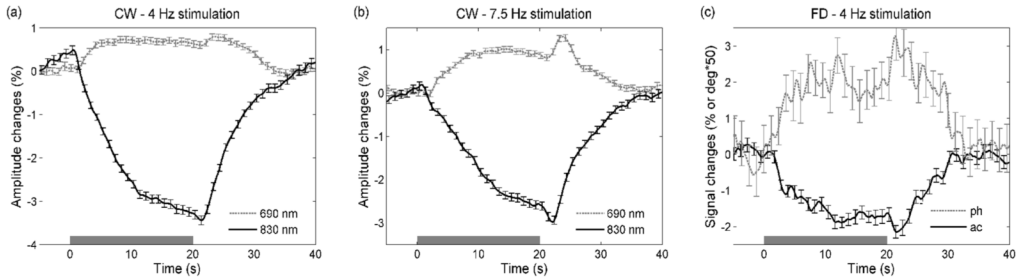

Figure 7.

Grand average of the slow optical responses (hemodynamic) for the CW measurements at 4Hz (panel a) and at 7.5Hz (panel b), and for the FD measurements at 4Hz (panel c). The error bars are standard errors. Please note that the y axis for the FD measurements is different. In the CW measurements the amplitude decreases at 830 nm because of the increase in absorption at 830 nm (HbO increase), and the amplitude increases at 690 nm because of the decrease in absorption at 690 nm (HbR decrease). Also, the FD ac at 830 nm decreases, and phase increases due to the absorption increase at that wavelength.

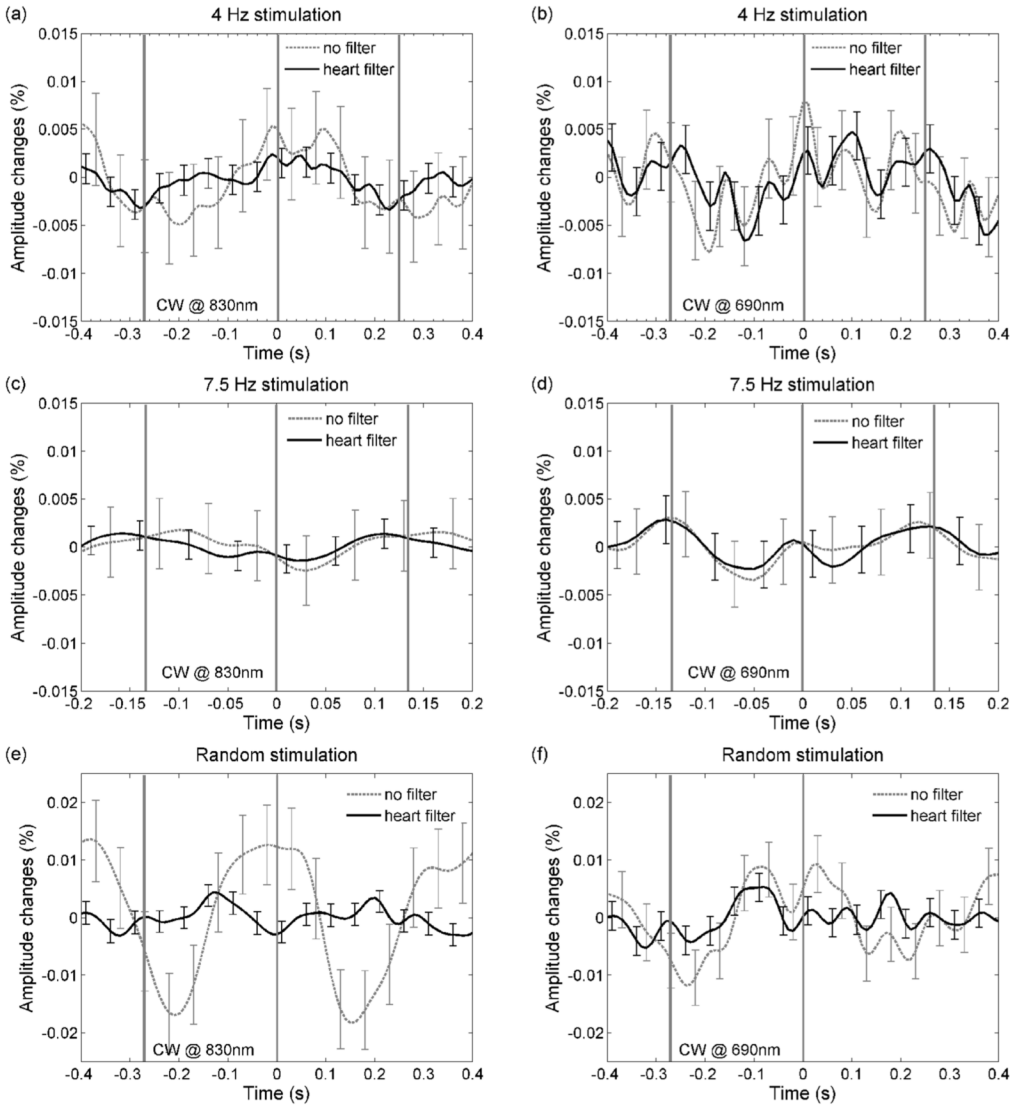

Figure 8.

Grand average of the fast amplitude responses for the CW measurements at 4Hz (panel a and b), at 7.5Hz (panel c and d), and for the random stimulation (panel e and f). The error bars are standard errors. The left panels show results at 830 nm, the right panels show results at 690 nm. In all graphs the results after applying the adaptive heart filter (black), and without applying the heart filter (dashed gray), are presented. While changes due to arterial pulsation are visible in some graphs, no significant changes with the fast signal periodicity are present.

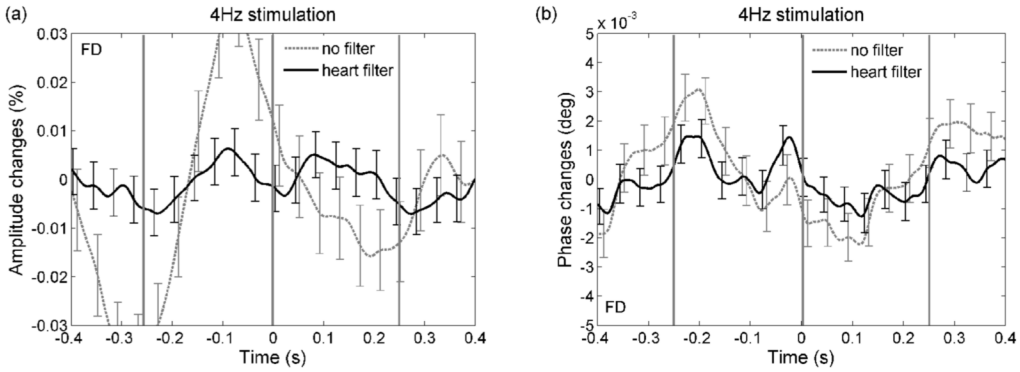

Figure 9.

Grand average of the fast amplitude (panel a) and phase shift (panel b) responses for the FD measurements at 4Hz. The error bars are standard errors. Black traces data after adaptive heart filter, dashed gray traces data without heart filter correction. Again, no significant changes with the fast signal periodicity are present.